Food Chemistry: X 17 (2023) 100574

Contents lists available at ScienceDirect

Food Chemistry: X

journal homepage: www.sciencedirect.com/journal/food-chemistry-x

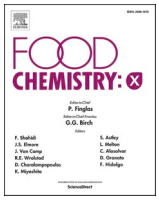

Further evaluation on structural and antioxidant capacities of soy protein isolate under multiple freeze–thaw cycles

Jiayue Wang [a], Zejian Xu [a], Lianzhou Jiang [a], Yan Zhang [b,*], Xiaonan Sui [a,*]

[a] College of Food Science, Northeast Agricultural University, Harbin 150030, China
[b] College of Horticulture and Landscape Architecture, Northeast Agricultural University, Harbin 150030, China

ARTICLE INFO

Keywords:
Soy protein isolate
Freeze thaw cycles
Precipitation
Structure analysis
Antioxidant capacity analysis

ABSTRACT

Multiple freeze–thaw (F–T) treatments could change a protein structure and affect its physicochemical activities. In this work, soy protein isolate (SPI) was subjected to multiple F–T treatments, and the changes in its physicochemical and functional properties were investigated. The three-dimensional fluorescence spectroscopy indicated that F–T treatments changed the structure of SPI, including an increase in surface hydrophobicity. Fourier transform infrared spectroscopy showed that SPI underwent denaturation, unfolding and aggregation due to the interchange of sulfhydryl-disulfide bonds and the exposure of hydrophobic groups. Correspondingly, the particle size of SPI increased significantly and the protein precipitation rate also increased from 16.69%/25.33% to 52.52%/55.79% after nine F–T treatments. The F–T treated SPI had a higher antioxidant capacity. Results indicate that F–T treatments may be used as a strategy to ameliorate preparation methods and improve functional characteristics of SPI, and suggest that multiple F–T treatment is an alternative way to recover soy proteins.

1. Introduction

Proteins are responsible for some of the most basic mechanisms of life, providing all essential functions for living organisms (Sui, Zhang, & Jiang, 2021). Soybean protein isolate (SPI) is generally derived from defatted soybean meal by alkali extraction and acid precipitation, and is one of the most significant and commercially-available soy protein products in the food industry (Zhao, Tian, Xu, Jiang, & Sui, 2023). SPIs have been recognized for their good nutritional value, favorable functional properties and beneficial health effects (Nishinari, Fang, Guo, & Phillips, 2014). The most commercially valuable SPI in the food industry is generally obtained by alkali extraction and acid precipitation from defatted soybean meal (Tang, 2017).

Due to the difficulties associated with transportation of food products over large distances, refrigeration is the most effective method used to inhibit the growth of microbes, thereby lengthening the quality guarantee period of general commodities (Zang et al., 2019). However, the repeated freeze–thaw (F–T) process will affect the quality of food products, in turn restricting the extensive development of food industry. For example, a process with multiple F–T cycles could result in denaturation, dissociation and possibly aggregation of individual egg white proteins via alteration of the sulfhydryl-disulfide interchange and surface hydrophobicity (Duan et al., 2017). The recrystallization of ice crystals and the changes in droplet microenvironment as a consequence of F–T cycles results in the destruction of the protein structure and effects the functional properties of proteins.

Processes with multiple F–T treatments are one of the more effective methods in modifying protein structures in order to improve the overall product function. For example, multiple F–T treatments can improve stability of soybean protein emulsion (Wang, Zhang, Wang, Xu, & Jiang, 2020). Existing research shows that SPI network subjected to F–T cycles was firmer, more uniform and more homogeneous and the stability of the Pickering nano-emulsion prepared by SPI was improved significantly through F–T treatments (Zhu et al., 2018). However, there are few studies on the structure and functional properties of pure SPI after multiple F–T cycles.

Therefore, the purpose of this study was to characterize the effect of a treatment process with multiple F–T cycles on the structures and functional characters of different concentrations SPI. The following characteristics of the processed products are studied: particle size, surface hydrophobicity, sulfhydryl group content, and the secondary and tertiary protein structure. Following which, antioxidant capacities of the

* Corresponding authors.
E-mail addresses: zhang_yan@neau.edu.cn (Y. Zhang), xiaonan.sui@neau.edu.cn (X. Sui).

https://doi.org/10.1016/j.fochx.2023.100574
Received 9 November 2022; Received in revised form 30 December 2022; Accepted 9 January 2023
Available online 10 January 2023

solutions were investigated. At the same time, the interactions between the functional and structural properties of proteins were further characterized. This study will allow for a better understanding of the interaction between form and function of proteins, providing a theoretical basis for the development of frozen food products.

2. Materials and methods

2.1. Materials

Soybeans (variety: Nong-Ken 42#) were purchased from Heilongjiang Academy of Agricultural Sciences (Harbin, Heilongjiang, China). 1-Anilino-8-naphthalene-sulphonate (ANS), 2,2-diphenyl-1-picrylhydrazyl (DPPH) and 2,2′-azinobis (3-ethylbenzothiazoline-6-sulphonic acid) (ABTS) were obtained from Sigma-Aldrich (St. Louis, MO, USA). Soybean oil was purchased from Jiusan Oil Co. Ltd. (Harbin, China).

2.2. Preparation of soy protein isolate

The production of SPI was conducted according to our previous work without any heat treatment (Zhang, Chen, Qi, Sui, & Jiang, 2018). Soybeans were crushed and sieved (60 mesh), and then mixed with *n*-hexane at a ratio of 1:5 thrice to degrease. The degreased soy powder was dissolved to 10 % (w/v) with DI water and kept at 45 °C for 2 h. Meanwhile, adjusted the pH of the mixture to 8.5 with 2 M NaOH. The mixture was then centrifuged immediately at 10,000*g* for 30 min. After removing the insoluble matter, the supernatant was collected and the pH was adjusted to 4.5 and then it was centrifuged at 6000*g* for 30 min to retrieve the precipitate. The dispersion was prepared using the precipitate dissolved in DI water at 15 % (w/v). Finally, the dispersion adjusted to pH 7.0, followed by lyophilizing to obtain SPI and storing in a desiccator.

2.3. Freeze-thaw treatment

The dispersion was prepared using SPI dissolved in PBS at 10 and 30 mg/mL. In order to completely hydrate the dispersion, stirred it on a magnetic stirrer at 4 °C for 12 h. Subsequently, the dispersion underwent a F–T cycles: frozen at −20 °C for 24 h, thawed at 20 °C for 8 h. The F–T treatment was repeated up to nine times, with an increment of two cycles. These samples would partially precipitate after freezing and thawing, therefore samples were centrifuged at 10,000*g* for 20 min, the supernatant stored at −4 °C for following analysis.

2.4. Protein concentration determination

After F–T treatments, the supernatant of samples was collected for protein concentration determination using Lowry's method. Lowry's reagent was obtained from Solarbio Technology Co., Ltd. (Beijing, China). Bovine serum albumin (BSA) was used as the standard.

2.5. Particle size measurement

Particle size measurements were conducted based on our previous study (Ding, Xu, Qi, Jiang, & Sui, 2018). The Mastersizer2000 (Malvern Instruments Co., Ltd., Worcestershire, UK) was used to measure the particle size of the supernatant of samples. Each sample was diluted in PBS buffer at 0.01 % (v/v) and stirred for 1 min on a magnetic stirring apparatus (IKA LAB DANCER, IKA-Werke GmbH and Co., Staufen, Germany) before testing. In addition, 1.456 and 1.333 were the refractive indices of the dispersed and continuous phases, respectively.

2.6. Free sulfhydryl groups measurement

The free sulfhydryl group (–SH) content of the supernatant of samples was measured according to the method of Li et al. (2018). The reaction solution samples were diluted to a protein concentration of 10 mg/mL with DI water. Next, the samples (1 mL) were dissolved in Tris-Gly buffer solution (5 mL) prepared with Tris (0.086 M), 0.09 mol/L glycine (0.09 M) and ethylenediaminetetraacetic acid (4 mM, pH 8.0). Then, 20 μL of Ellman's reagent solution (1.0 mM 5,5′-dithio-bis-2-nitrobenzoic acid) was mixed with the above solution, and The mixture was shook for 15 min at 25 °C in the dark to mix well. The value at the wavelength of 412 nm was recoded. The sample without Ellman's reagent was used as the control. The content of –SH was calculated using Eq. (1).

$$-\mathrm{SH}(\mu\mathrm{mol}/\mathrm{g}) = \frac{73.53 \times A_{412} \times \mathrm{D}}{\mathrm{C}} \quad (1)$$

where A_{412} represents the absorbance at 412 nm; C represents the content of solids in protein solution (mg/mL); and D represents the dilution factor.

2.7. Surface hydrophobicity measurement

ANS^{-} was used as the fluorescence probe to measure surface hydrophobicity (H_0) (Kohler, Santana, Braisch, Preis, & Schuchmann, 2010). Briefly, the supernatant of each sample was diluted to a range of 0.05 to 2.0 mg/mL in PBS. Aliquots (20 μL) of ANS (8.0 mM) were prepared using PBS and then added to 4 mL of each protein solution. A 96-well plate containing 200 μL of mixed solution per well was rested with Tecan Infinite M200 microplate reader for 15 min in the dark (Tecan Inc., Maennedorf, Switzerland) at excitation and emission wavelengths of 390 and 470 nm, respectively. The slit width was set to 5 nm. The slope of the graph of fluorescence intensity versus protein concentration was H_0.

2.8. Fluorescence spectroscopy measurement

Fluorescence spectroscopy was conducted according to the method reported by Sui et al. (2018). The F-4500 fluorescence spectrophotometer (Hitachi Co., Tokyo, Japan) was used to perform the intrinsic fluorescence emission spectra of protein samples. The supernatant of samples with concentrations of 10 and 30 mg/mL were first diluted with PBS to 0.2 mg/mL. Excitation (Ex) using three-dimensional fluorescence was initiated using a wavelength of 200 nm (Increment of 10 nm), and the recorded emission (Em) wavelength set 200 to 500 nm. The slit width was set to 5 nm. The intrinsic fluorescence spectra of SPI through multiple F–T treatment were also recorded for analysis using an Origin 2017 software (OriginLab, Northampton, MA, USA).

2.9. Fourier transform infrared spectroscopy

The secondary structures of the supernatant of samples were analyzed and infrared spectra were recorded using a FTIR spectrometer (Nicolet 6700, Thermo Nicolet Company, USA). Before FTIR analysis, the F–T sample was freeze-dried. The resulting freeze-dried sample was laminated with KBr at 1:100 (w/w), ground into powder, and pressed into tablets at 20 MPa.

2.10. Measurement of antioxidant capacity

DPPH and $ABTS^{\bullet+}$ methods were adopted to determine the antioxidant capacity of samples. A microplate reader was used in both assays. Sample solutions for testing were prepared by dispersing in PBS prior to measurement.

2.10.1. DPPH radical scavenging activity assay

The DPPH radical scavenging activity was performed based on the method of Sridhar and Charles (2019). DPPH stock solution with a

concentration of 0.1 mM was prepared by dissolving DPPH powder in 95 % methanol. In each well, an aliquot of 100 μL of the supernatant of each sample solution was added to an equal volume of DPPH stock solution and incubated in the dark at ambient temperature for 30 min. The same microplate reader was used to measure the absorbance of the mixture at 517 nm. Equal volume PBS replaced the sample as the black. Using Eq. (2) to calculate the DPPH radical scavenging activity.

$$DPPH\ radical\ scavening\ activity(\%) = [(A_b - A_s)/A_b] \times 100 \quad (2)$$

where, As and A_b represent the absorbance of sample and blank.

2.10.2. $ABTS^{\bullet+}$ method

The $ABTS^{\bullet+}$ radical scavenging activity assay was conducted based on our previous study using 96-well microplates (Ju et al., 2020). The $ABTS^{\bullet+}$ solution was prepared by ABTS (7.0 mM) mixed with potassium persulfate (2.4 mM) prior to the analysis and left to react and keep in the dark place for 12–16 h. The $ABTS^{\bullet+}$ solution was added to PBS to be diluted and made the absorbance at 734 nm reach at the range of 0.68–0.72, subsequently. Aliquots of 10 μL supernatant of the sample solutions was mixed with 90 μL of the diluted $ABTS^{\bullet+}$ solution left to react for 7 min in the dark. The absorbance was measured using the same microplate reader at the wavelength of 734 nm. Equal volume PBS replaced the sample as the blank. Using Eq. (3) to calculate the $ABTS^{\bullet+}$ radical scavenging activity.

$$ABTS^{\bullet+}radicalscaveningactivity(\%) = [(A_b - A_s)/A_b] \times 100 \quad (3)$$

where A_s and A_b represent the absorbance of sample and blank.

2.11. Statistical analysis

Each measurement was performed in triplicates and the results were expressed as mean ± SD. Statistical analysis was performed using one-way analysis of variance (ANOVA) and Duncan's test ($p < 0.05$) using the SPSS software (SPSS Inc., Evanston, IL).

3. Results and discussion

3.1. Protein concentration analysis

In most cases, the functional properties of SPI are closely related to its concentration. As such, it is regarded as one of the main indicators to measure in order to determine the physical and functional properties of proteins. An example of samples after multiple F–T treatments is shown in the top figures of Fig. 1. Results obtained indicated that F–T treatments led to SPI precipitation, which was more pronounced with increasing F–T cycles. The protein concentration in the aqueous phase (AP) and protein precipitation rate after one, three, five, seven, and nine F–T cycles is presented in Table 1. As shown in Table 1, both 10 mg/mL and 30 mg/mL of protein concentrations showed the same trend in results. Compared to the control, the precipitation rate increased significantly after F–T treatments and reached the highest values of 52.52 and

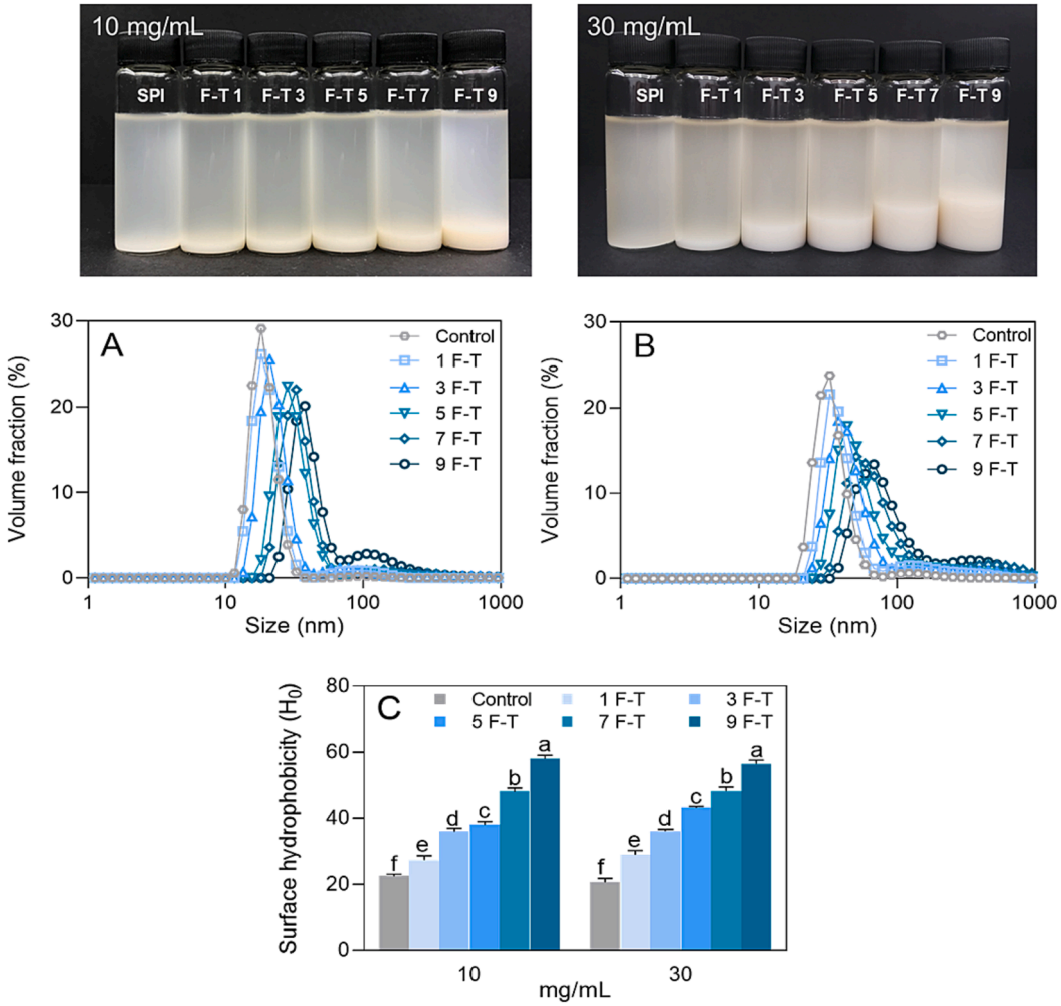

Fig. 1. Particle size analysis of SPI solution of 10 (A) and 30 (B) mg/mL after different F–T cycles. An example of samples (Top figures). (C) Surface hydrophobicity (H_0) analysis of SPI solution after different F–T cycles. Different letters (a–f) in the same concentration of protein indicate significant differences.

Table 1
Precipitation rate and protein concentrations.

F–T cycles	Precipitation rate (%)		Protein concentration (mg/mL)	
	10 mg/mL	30 mg/mL	10 mg/mL	30 mg/mL
Control	16.69 ± 1.24^{e}	25.33 ± 0.38^{e}	8.33 ± 0.12^{a}	22.39 ± 0.11^{a}
1 F–T	23.11 ± 1.30^{d}	29.26 ± 0.49^{d}	7.68 ± 0.13^{b}	21.22 ± 0.14^{b}
3 F–T	29.69 ± 0.99^{c}	32.87 ± 0.93^{c}	7.03 ± 0.09^{c}	20.13 ± 0.27^{c}
5 F–T	30.19 ± 1.32^{c}	34.56 ± 0.35^{c}	6.98 ± 0.13^{c}	19.63 ± 0.11^{c}
7 F–T	33.85 ± 2.16^{b}	38.37 ± 1.07^{b}	6.61 ± 0.21^{d}	18.48 ± 0.32^{d}
9 F–T	52.52 ± 0.81^{a}	55.79 ± 2.44^{a}	4.74 ± 0.08^{e}	13.26 ± 0.73^{e}

Values are given as means ± SD. Different letters (a–e) in the same column indicate significant differences ($P < 0.05$).

55.79 % after the completion of nine F–T cycles. The initial protein concentrations of the different control solutions (10 and 30 mg/mL) were 8.33 and 22.39 mg/mL respectively, both of which decreased significantly to 4.74 and 13.26 mg/mL as the samples underwent nine F–T cycles. The results of protein concentration test in the AP showed that the concentration decreased as the number of F–T cycles increased. Cao, Chen, Cui, and Foster (2003) found that freezing could induce several stresses that resulted in the denaturation of proteins, such as the formation of ice crystals, the co-crystallization of solutes and buffer solutes caused by water crystallization. The denatured protein molecules would further combine into aggregates or even precipitate, resulting in poor solubility (Tang, Wang, Yang, & Li, 2009). Moreover, the recrystallization of ice due to water redistribution contributed to the disruption of protein network. Ice crystals formed during freezing drives ice recrystallization which possibly resulted in further destruction of the hydrophobic interactions, the disulfide bonds and the hydrogen bond that were the main forces of of interaction within and between protein molecules (Harnkarnsujarit, Kawai, & Suzuki, 2015), resulting in the protein entering an unstable state. The research of Zhu, Li, Zhao, Song, and Li (2019) also indicated that the structure of gluten became more irregular after F–T. The molecular conformation of gluten proteins would be rearranged to the minimum-energy state to keep them relatively stable when exposed to the new frozen environment (Wang, Jin, & Xu, 2015). Therefore, the concentration of SPI was significantly reduced after F–T treatment. In addition, the precipitation rate after ten F–T cycles was also measured in this study. While this did not increase significantly, it may continue to increase as the number of F–T cycles increases. In this case, such aggregation and precipitation which were generally considered negative phenomena, could provide tools for further recovery of soluble proteins in the classical pH-shift process.

3.2. Particle size analysis

The particle size distribution is a vital parameter for evaluating the evenness index of a protein solution, and it is closely related to the physicochemical and functional properties of the solution (McClements, 1996). The impact of F–T treatment on the particle size of the supernatant of different concentrations of SPI solution was measured. As shown in Fig. 1, (A) and (B) show the particles sizes of 10 and 30 mg/mL of protein solutions, respectively. It was observed that the volume particle size of SPI solutions after different F–T cycles gradually increased in comparison to SPI and the particle size distribution peak gradually shifted to bigger sizes. Noshad, Mohebbi, Shahidi, and Koocheki (2015) reported that the particles size of SPI emulsions increased significantly with the number of F–T cycles increased. It was suggested that that the formation of larger particles could be attributed mainly to the extensive droplet aggregation that occurred in the emulsion after the F–T cycle. It was previously reported that egg phosvitin underwent denaturation, dissociation and possibly aggregation after three, six, and nine F–T cycles (Li et al., 2018). In Fig. 1A-B, it could be observed that an increase of SPI concentration from 10 to 30 mg/mL resulted in the increase of overall particle size. In addition, it was also found that the particle size distributions of the control groups of 10 and 30 mg/mL protein solutions both displayed great monodispersity, but a multi-peak state was observed in the protein solution subjected to multiple F–T treatments. Although there were fewer particles with larger diameters, it had a greater impact on the total volume of the system. Zang et al. (2019) found that the particle size of the oil/water emulsion prepared with papain and transglutaminase-modified soy protein isolates increased significantly as the F–T cycle increased. Therefore, the increase in particles size might be due to protein denaturation or aggregation after the F–T cycles. Results obtained in Section "3.1" further confirmed the observations noted in this section.

3.3. Exposed sulfhydryl groups analysis

Sulfhydryl groups are the among the most active groups in proteins and can significantly affect the functional properties of proteins. The effect of F–T treatment on the exposed sulfhydryl groups of various concentration proteins (10 and 30 mg/mL) was studied. Results obtained are shown in Table 2. The concentration of exposed sulfhydryl groups in the F–T SPI solution gradually decreased as the number of F–T cycles increased. This was consistent the findings by Wang et al. (2020), who studied the variation trend of the sulfhydryl content of freeze-thawed egg yolks. Such differences in exposed sulfhydryl content might be due to the preparation methods and F–T cycle times of protein. Noh, Park, Pak, Hong, and Yun (2005) proposed that the soy protein solution would form intermolecular disulfide bonds in the frozen state. Interestingly, there was no significant difference of the content of exposed sulfhydryl groups between control and one F–T cycle, three and five F–T cycles, but when subjected to seven and nine F–T cycles decreased with the increase of F–T cycles. Exposed sulfhydryl content of proteins (10 and 30 mg/mL) was reduced from 7.55 ± 0.39 and 6.26 ± 0.08 μmol/g to 4.33 ± 0.21 and 2.92 ± 0.11 μmol/g when the number of F–T cycles increased from zero to nine, respectively, corresponding to significant reductions of 42.64 % and 53.35 % ($P < 0.05$). Similar to the observed trend of protein solubility, the exposed sulfhydryl content of all samples decreased significantly. During F–T treatment of proteins or their products, the reduction in sulfhydryl groups was due to the formation of disulfide bonds or disulfide bonds interchanges induced by oxidation (Leelapongwattana, Benjakul, Visessanguan, & Howell, 2005). In other words, the hydrogen bonds of water molecules were disrupted by the F–T treatment, and the balance between the water-bound sulfhydryl groups and the exposed sulfhydryl groups on the protein surface also changed, resulting in a decrease in the content of exposed sulfhydryl groups. The phenomenon of reduction of the content of exposed sulfhydryl groups by F–T processing of proteins was also observed by Yasemi (2017). At the same time, the decrease in sulfhydryl content might also be due to the masking of sulfhydryl groups caused by protein aggregation.

3.4. Surface hydrophobicity (H_0) analysis

The number of hydrophobic groups on the surface is represented by

Table 2
Content of exposed sulfhydryl (-SH) groups of SPI under different F–T cycles.

F–T cycles	Exposed sulfhydryl (μmol/g)	
	10 mg/mL	30 mg/mL
Control	7.55 ± 0.39^{a}	6.26 ± 0.08^{a}
1 F–T	7.01 ± 0.17^{ab}	5.91 ± 0.12^{a}
3 F–T	6.54 ± 0.59^{b}	5.27 ± 0.42^{b}
5 F–T	6.39 ± 0.34^{b}	5.26 ± 0.23^{b}
7 F–T	4.88 ± 0.24^{c}	2.96 ± 0.29^{c}
9 F–T	4.33 ± 0.21^{c}	2.92 ± 0.11^{c}

Values are given as means ± SD. Different letters (a–c) in the same column indicate significant differences ($P < 0.05$).

H_0. The hydrophobic region formed by non-polar residues on the surface of the protein could be combined with fluorescent probes (ANS). As shown in Fig. 1C. H_0 value of the 10 and 30 mg/mL SPI solution both increased significantly after multiple F–T cycles compared to that of untreated SPI. The protein solution after nine F–T cycles showed the highest H_0 value. The freezing treatment resulted in a clearly increase of the surface hydrophobicity of soy proteins, which indicated that the freezing of soy protein caused the conformation of soy protein to be changed (Noh, Kang, Hong, & Yun, 2006). This could be due to some hydrophobic regions of SPI that were previously located buried within the interior of the molecules being redistributed and exposed on the outside the protein molecules, resulting in an increase in H_0. (Hu, Lichan, Wan, Tian, & Pan, 2013). Another analysis for this trend could be due to the unfolding, which increased the count of sites on the protein surface that can be used to bind fluorescent probes (Li et al., 2016). During this F–T process, surface hydrophobicity increased and was inversely correlated with the free sulfhydryl groups. SPI powder was oxidized during the food processing, resulting in increased surface-exposed hydrophobicity and decreased exposed sulfhydryl (Duqueestrada, Kyriakopoulou, De Groot, Der Goot, & Bertoncarabin, 2020). Duan et al. (2017) obtained similar results in their word focusing on ovomucoid. They proposed that the increased surface hydrophobicity was derived from molecular rearrangement with exposure of hydrophobic side chain groups. This result indicated that the repeated cycles of the F–T treatment exposed the protein hydrophobic groups.

3.5. Fluorescence spectroscopy analysis

Three-dimensional (3D) fluorescence spectroscopy is a well-established and effective method to study the three-dimensional structure of proteins (Ding, Liu, Li, Zhang, & Sun, 2010). The changes in protein characteristics and conformation were explored by observing the double-scan images of Fig. 2. Peak a ($\lambda_{ex} = \lambda_{em}$) and Peak b ($2\lambda_{ex} = \lambda_{em}$) represent the first-order diffraction peak of the Rayleigh scattering and the second-order diffraction peak, respectively (Sui et al., 2018). Peak 1 ($\lambda_{ex} = 280$ nm, $\lambda_{em} = 340$ nm) mainly characterizes the polarity of the surrounding environment that tryptophan and tyrosine are highly dependent on. As shown in Fig. 2, the fluorescence value of protein Peak 1 of both 10 and 30 mg/mL SPI reduced after multiple F–T cycles. The fluorescence intensity of 10 and 30 mg/mL SPI was lowest at the end of nine F–T cycles. Meanwhile, the concentration of SPI was found to be proportional to the fluorescence value at protein Peak 1 under the same number of F–T cycles. The phenomenon indicated that the structure of SPI might change as the number of F–T cycle increases, resulting in more tryptophan and tyrosine residues being exposed to a hydrophilic environment. The fluorescence values of tryptophan and tyrosine decreased

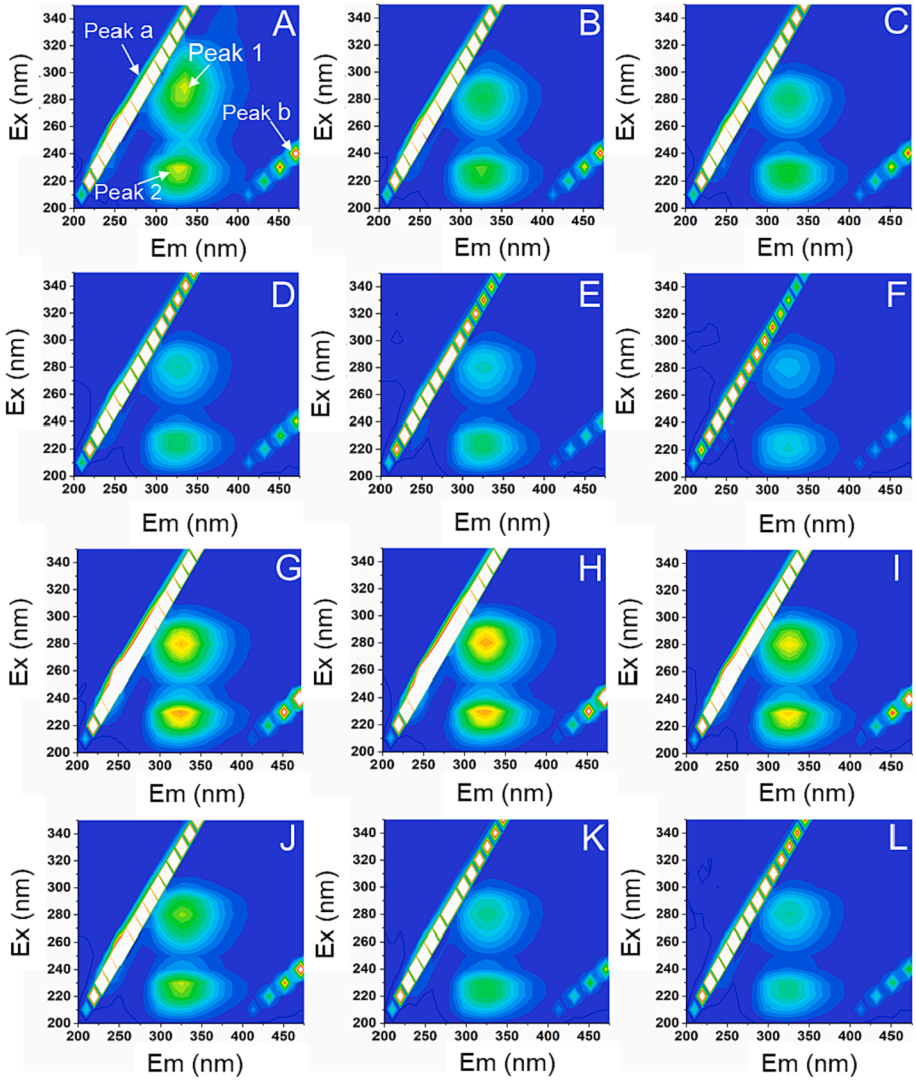

Fig. 2. Three-dimensional fluorescence spectra maps of 10 mg/mL (A: control; B:1 F–T; C:3 F–T; D:5 F–T; E:7 F–T; F:9 F–T) and 30 mg/mL (G: control; H:1 F–T; I:3 F–T; J:5 F–T; K:7 F–T; L:9 F–T) SPI solutions after multiple F–T cycles.

with exposure to the hydrophilic environment (Jiang et al., 2019). As the concentration of SPI increased, the fluorescence value decreased to an even greater extent. In addition, Peak 2 ($\lambda_{ex} = 230$ nm, $\lambda_{em} = 350$ nm) in Fig. 2 mainly represented the characteristic peak of the polypeptide chain backbone (Ding et al., 2010). After 10 and 30 mg/mL SPI undergoing multiple F–T cycles, the fluorescence value at Peak 2 of the samples decreased as the number of F–T cycles increased. Pallarès, Vendrell, Avilés, and Ventura (2004) pointed out that the unfolding of the protein structure would cause more chromophores to be exposed to the solvent, which would be considered as the cause of the decrease in fluorescence intensity. Therefore, this indicated that the F–T cycle unfolded the SPI polypeptide chain, which changed the tertiary structure of the protein.

3.6. Fourier transforms infrared spectrometer analysis

FTIR spectroscopy is an effective way to measure sensitive changes in the protein secondary structure (Farhat, Orset, Moreau, & Blanshard, 1998). Three different absorption bands of Amide I, Amide II and Amide III bands constitute the FTIR spectrum. This method was used to characterize 10 and 30 mg/mL SPI under various F–T cycles in order to obtain a quantitative determination of protein secondary structure (Fig. 3A-B). The Amide I band was currently used for quantitative analysis of protein secondary structure, mainly arised from the stretching of C═O. The presence of α-helix (1649–1661 cm^{-1}), β-sheet (1611–1634 and 1681–1700 cm^{-1}), β-turn (1665–1680 cm^{-1}), and random coil (1635–1648 cm^{-1}) were included in the Amide I. As shown in Fig. 3A-B, the peak intensity of the Amide I band decreased for both 10 and 30 mg/mL SPI samples, with an increase in the number of F–T cycles. The absorbance of samples at the Amide I band decreased, indicating that it may be due to the rearrangement of protein peptide chains resulted from F–T treatment and with a corresponding change in the secondary structure (Nanda, Sarkar, & Banerjee, 2007). In addition, a slight red shift could be seen from the Amide I band. To further characterize the changes in the secondary structure, quantitative estimations of various structural conformations were determined and

Table 3
The contents of secondary structure of 10 and 30 mg/mL SPI subjected to treatment with differing F–T cycles.

Samples	Content (%)			
	α-helix	β-sheet	β-turn	Random coil
10 mg/mL				
Control	18.95 ± 0.72^{a}	36.33 ± 0.52^{c}	22.54 ± 0.34^{a}	22.16 ± 0.90^{b}
1 F–T	17.76 ± 0.42^{b}	37.72 ± 0.53^{b}	21.45 ± 0.83^{ab}	23.05 ± 0.94^{b}
3 F–T	17.32 ± 0.43^{b}	38.21 ± 0.23^{b}	20.94 ± 1.43^{b}	23.51 ± 1.20^{b}
5 F–T	16.72 ± 0.42^{b}	38.39 ± 0.78^{ab}	20.34 ± 0.97^{b}	24.53 ± 1.19^{ab}
7 F–T	16.07 ± 0.33^{c}	39.16 ± 0.52^{ab}	20.20 ± 0.47^{b}	24.55 ± 0.67^{ab}
9 F–T	15.70 ± 0.38^{d}	39.42 ± 0.95^{a}	19.77 ± 0.26^{b}	25.12 ± 0.85^{a}
30 mg/mL				
Control	19.13 ± 0.47^{A}	37.28 ± 0.49^{B}	21.71 ± 0.28^{A}	21.86 ± 0.24^{C}
1 F–T	18.51 ± 0.81^{AB}	37.53 ± 1.05^{B}	21.12 ± 0.31^{AB}	22.82 ± 0.55^{B}
3 F–T	18.26 ± 0.29^{B}	37.88 ± 1.45^{AB}	21.06 ± 0.77^{AB}	22.78 ± 1.76^{B}
5 F–T	17.42 ± 0.57^{B}	38.27 ± 1.92^{AB}	20.48 ± 0.94^{B}	23.81 ± 0.88^{AB}
7 F–T	16.45 ± 0.58^{B}	38.45 ± 0.53^{AB}	20.30 ± 0.79^{B}	24.78 ± 0.74^{AB}
9 F–T	16.10 ± 0.60^{B}	39.70 ± 1.09^{A}	19.70 ± 0.59^{B}	24.53 ± 0.82^{A}

Values are given as means ± SD. Different letters (a–c/A-C) in the same column indicate significant differences ($P < 0.05$).

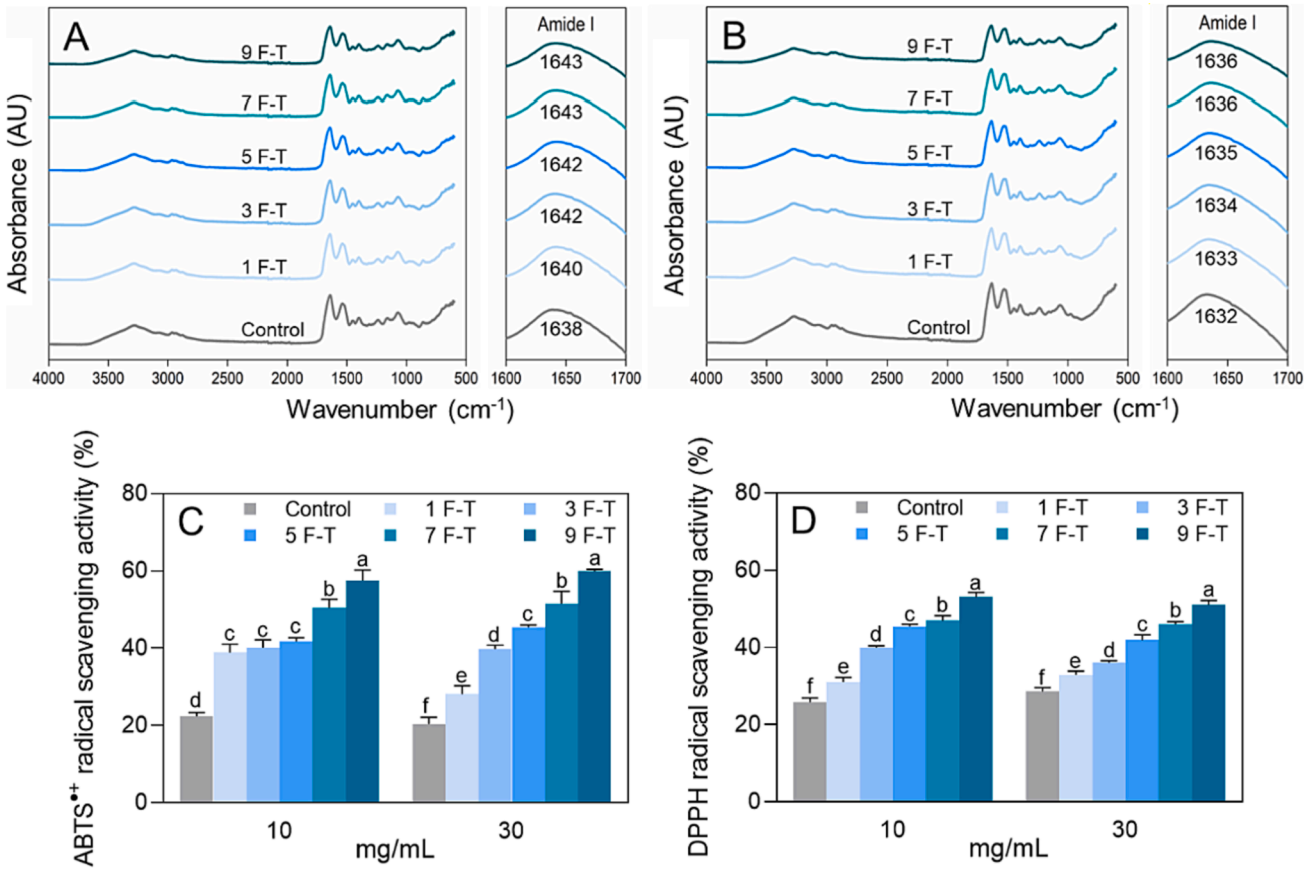

Fig. 3. FTIR spectra of SPI solution of 10 (A) and 30 (B) mg/mL after different F–T cycles. Antioxidant capacity of SPI solution of 10 (C) and 30 (D) mg/mL after different F–T cycles.

results are shown in Table 3. Interestingly, there was a significant decrease in α-helix and β-turn with increasing F–T cycles, with a corresponding increase in β-sheet and random coil content. The results shown in Table 3 indicated that α-helix, β-turn, β-sheet and random coil were more sensitive to temperature fluctuations during the F–T cycles. The decrease in α-helix that was the highly ordered structural conformation indicated that the structure of SPI became unfolded and tended towards to a disordered state such that the proportion of random coil increased. Kong and Yu (2007) proposed that the molecular structure of the protein was relatively loose when the content of β-sheets and random coils changed opposite to α-helix in the protein, with the hydrophobic situated in the protein being exposed in large quantities, thus showing greater surface hydrophobicity. This is consistent with results reported in Section "3.1". Similar observations were also noted in hydrated gluten during F–T cycles. Esselink, Van Aalst, Maliepaard, and Van Duynhoven (2003) found the rearrangement of the protein spatial conformation during cryopreservation was arised from the interaction between covalent and non-covalent bonds (such as hydrophobic interaction). As such, the results indicated that the F–T treatment could change the secondary structure of SPI.

3.7. Antioxidant capacity analysis

Fig. 3C-D shows antioxidant capacity activities of the 10 and 30 mg/mL SPI after treatments with differing F–T cycles. Studies showed that physical and chemical processing methods of SPI could enhanced its antioxidant capacity (Liu & Zhao, 2010). In this study, the controls of both 10 mg/mL and 30 mg/mL SPI exhibited relatively weak antioxidant activities, with only 25.5 % and 28.6 % of DPPH radical scavenged, and 22.3 % and 20.3 % of $ABTS^{\bullet+}$ scavenged, respectively. Sample processing involving any number of F–T cycles resulted in an significant increase in the antioxidant activities of both 10 and 30 mg/mL SPI. The free radical scavenging capacity of the SPI sample on DPPH increased to approximately 53 % and 51 %, while $ABTS^{\bullet+}$ radical scavenging capacity increased to approximately 57 % and 59 %, respectively. Zhang, Shan, Hong, Luo, and Ye (2020) found that freeze-thawed bighead carp had strong antioxidant activity. For both antioxidant capacity assays, SPI samples at 10 and 30 mg/mL showed significantly higher antioxidant capacity after nine F–T cycles compared with a fewer cycles. Results obtained indicated that multiple F–T cycles could be used to enhance the antioxidant capacity of SPI and that the F–T-treated SPI solutions might even be used as a potential source of antioxidants.

4. Conclusion

The physicochemical properties of SPI that had undergone multiple F–T cycles were studied. These results showed the secondary structure of SPI changed after multiple F–T cycles, which in turn resulted in changes to the molecular arrangement and interaction, thereby unfolding the protein to form aggregates, leading to increased particle sizes, decreased solubility, and a significantly improved antioxidant activity and surface hydrophobicity. Redistribution of water, recrystallization of ice and mechanical damage of protein molecules during the F–T treatment led to the depolymerization of SPI. This study provided an effective theoretical basis for the development of frozen foods containing SPI and other soy-based ingredients.

CRediT authorship contribution statement

Jiayue Wang: Conceptualization, Methodology, Software, Writing – original draft. **Zejian Xu:** Conceptualization, Methodology, Software, Writing – original draft. **Lianzhou Jiang:** Visualization, Investigation. **Yan Zhang:** Visualization, Investigation. **Xiaonan Sui:** Supervision, Writing – review & editing.

Declaration of Competing Interest

The authors declare that they have no known competing financial interests or personal relationships that could have appeared to influence the work reported in this paper.

Data availability

Data will be made available on request.

Acknowledgement

We gratefully acknowledge the financial support received from the Excellent Young Scientists Fund of National Science Foundation of China (32022068) and the Key Program of NSFC (U22A20548).

References

Cao, E., Chen, Y., Cui, Z., & Foster, P. R. (2003). Effect of freezing and thawing rates on denaturation of proteins in aqueous solutions. *Biotechnology and Bioengineering, 82*(6), 684–690.

Ding, F., Liu, W., Li, N., Zhang, L., & Sun, Y. (2010). Complex of nicosulfuron with human serum albumin: A biophysical study. *Journal of Molecular Structure, 975*(1–3), 256–264.

Ding, J., Xu, Z., Qi, B., Jiang, L., & Sui, X. (2018). Physicochemical and oxidative stability of a soybean oleosome-based emulsion and its in vitro digestive fate as affected by (−)-epigallocatechin-3-gallate. *Food & Function, 9*(12), 6146–6154.

Duan, X., Li, J., Zhang, Q., Zhao, T., Li, M., Xu, X., & Liu, X. (2017). Effect of a multiple freeze-thaw process on structural and foaming properties of individual egg white proteins. *Food Chemistry, 228*, 243–248.

Duqueestrada, P., Kyriakopoulou, K., De Groot, W., Der Goot, A. J. V., & Bertoncarabin, C. C. (2020). Oxidative stability of soy proteins: From ground soybeans to structured products. *Food Chemistry, 318*, Article 126499.

Esselink, E. F. J., Van Aalst, H., Maliepaard, M., & Van Duynhoven, J. P. (2003). Long-term storage effect in frozen dough by spectroscopy and microscopy. *Cereal Chemistry, 80*(4), 396–403.

Farhat, I. A., Orset, S., Moreau, P., & Blanshard, J. M. (1998). FTIR study of hydration phenomena in protein–sugar systems. *Journal of Colloid and Interface Science, 207*(2), 200–208.

Harnkarnsujarit, N., Kawai, K., & Suzuki, T. (2015). Effects of freezing temperature and water activity on microstructure, color, and protein conformation of freeze-dried bluefin tuna (Thunnus orientalis). *Food and Bioprocess Technology, 8*(4), 916–925.

Hu, H., Lichan, E. C. Y., Wan, L., Tian, M., & Pan, S. (2013). The effect of high intensity ultrasonic pre-treatment on the properties of soybean protein isolate gel induced by calcium sulfate. *Food Hydrocolloids, 32*(2), 303–311.

Jiang, L., Liu, Y., Li, L., Qi, B., Ju, M., Xu, Y., … Sui, X. (2019). Covalent conjugates of anthocyanins to soy protein: Unravelling their structure features and in vitro gastrointestinal digestion fate. *Food Research International, 120*, 603–609.

Ju, M., Zhu, G., Huang, G., Shen, X., Zhang, Y., Jiang, L., & Sui, X. (2020). A novel pickering emulsion produced using soy protein-anthocyanin complex nanoparticles. *Food Hydrocolloids, 99*, Article 105329.

Kohler, K., Santana, A. S., Braisch, B., Preis, R., & Schuchmann, H. P. (2010). High pressure emulsification with nano-particles as stabilizing agents. *Chemical Engineering Science, 65*(10), 2957–2964.

Kong, J., & Yu, S. (2007). Fourier transform infrared spectroscopic analysis of protein secondary structures. *Acta Biochimica et Biophysica Sinica, 39*(8), 549–559.

Leelapongwattana, K., Benjakul, S., Visessanguan, W., & Howell, N. K. (2005). Physicochemical and biochemical changes during frozen storage of minced flesh of lizardfish (Saurida micropectoralis). *Food Chemistry, 90*(1), 141–150.

Li, M., Li, X., Li, J., Lu, M., Liu, X., & Duan, X. (2018). Effects of multiple freeze–thaw treatments on physicochemical and biological activities of egg phosvitin and its phosphopeptides. *Food & Function, 9*(9), 4602–4610.

Li, W., Zhao, H., He, Z., Zeng, M., Qin, F., & Chen, J. (2016). Modification of soy protein hydrolysates by Maillard reaction: Effects of carbohydrate chain length on structural and interfacial properties. *Colloids and Surfaces B: Biointerfaces, 138*, 70–77.

Liu, T. X., & Zhao, M. (2010). Physical and chemical modification of SPI as a potential means to enhance small peptide contents and antioxidant activity found in hydrolysates. *Innovative Food Science & Emerging Technologies, 11*(4), 677–683.

McClements, D. J. (1996). Principles of ultrasonic droplet size determination in emulsions. *Langmuir, 12*(14), 3454–3461.

Nanda, R. K., Sarkar, N., & Banerjee, R. (2007). Probing the interaction of ellagic acid with human serum albumin: A fluorescence spectroscopic study. *Journal of Photochemistry Photobiology A Chemistry, 192*(2–3), 152–158.

Nishinari, K., Fang, Y., Guo, S., & Phillips, G. O. (2014). Soy proteins: A review on composition, aggregation and emulsification. *Food Hydrocolloids, 39*, 301–318.

Noh, E. J., Kang, C., Hong, S. T., & Yun, S. E. (2006). Freezing of soybeans influences the hydrophobicity of soy protein. *Food Chemistry, 97*(2), 212–216.

Noh, E. J., Park, S. Y., Pak, J. I., Hong, S. T., & Yun, S. E. (2005). Coagulation of soymilk and quality of tofu as affected by freeze treatment of soybeans. *Food Chemistry, 91*(4), 715–721.

Noshad, M., Mohebbi, M., Shahidi, F., & Koocheki, A. (2015). Freeze–thaw stability of emulsions with soy protein isolate through interfacial engineering. *International Journal of Refrigeration-revue Internationale Du Froid, 58*, 253–260.
Pallarès, I., Vendrell, J., Avilés, F. X., & Ventura, S. (2004). Amyloid fibril formation by a partially structured intermediate state of α-chymotrypsin. *Journal of Molecular Biology, 342*(1), 321–331.
Wang, R., Ma, Y., Ma, Z., Du, Q., Zhao, Y., & Chi, Y. (2020). Changes in gelation, aggregation and intermolecular forces in frozen-thawed egg yolks during freezing. *Food Hydrocolloids, 105947*.
Sridhar, K., & Charles, A. L. (2019). In vitro antioxidant activity of Kyoho grape 527 extracts in DPPH and ABTS assays: Estimation methods for EC50 using 528 advanced statistical programs. *Food Chemistry, 275*, 41–49.
Sui, X., Sun, H., Qi, B., Zhang, M., Li, Y., & Jiang, L. (2018). Functional and conformational changes to soy proteins accompanying anthocyanins: Focus on covalent and non-covalent interactions. *Food Chemistry, 245*, 871–878.
Sui, X., Zhang, T., & Jiang, L. (2021). Soy protein: Molecular structure revisited and recent advances in processing technologies. *Annual Review of Food Science and Technology, 12*(1), 119–147.
Tang, C. H., Wang, X. Y., Yang, X. Q., & Li, L. (2009). Formation of soluble aggregates from insoluble commercial soy protein isolate by means of ultrasonic treatment and their gelling properties. *Journal of Food Engineering, 92*(4), 432–437.
Tang, C. H. (2017). Emulsifying properties of soy proteins: A critical review with emphasis on the role of conformational flexibility. *Critical Reviews in Food Science and Nutrition, 57*(12), 2636–2679.
Wang, P., Jin, Z., & Xu, X. (2015). Physicochemical alterations of wheat gluten proteins upon dough formation and frozen storage–A review from gluten, glutenin and gliadin perspectives. *Trends in Food Science & Technology, 46*(2), 189–198.
Wang, Y., Zhang, A., Wang, X., Xu, N., & Jiang, L. (2020). The radiation assisted-Maillard reaction comprehensively improves the freeze-thaw stability of soy protein-stabilized oil-in-water emulsions. *Food Hydrocolloids, 103*, Article 105684.
Yasemi, M. (2017). Prevention of denaturation of freshwater crayfish muscle subjected to different freeze-thaw cycles by gelatin hydrolysate. *Food Chemistry, 234*, 199–204.
Zang, X., Liu, P., Chen, Y., Wang, J., Yu, G., & Xu, H. (2019). Improved freeze-thaw stability of o/w emulsions prepared with soybean protein isolate modified by papain and transglutaminase. *LWT, 104*, 195–201.
Zhao, Y., Tian, R., Xu, Z., Jiang, L., & Sui, X. (2023). Recent advances in soy protein extraction technology. *Journal of the American Oil Chemists' Society*. https://doi.org/10.1002/aocs.12676
Zhang, L., Shan, Y., Hong, H., Luo, Y., & Ye, W. (2020). Prevention of protein and lipid oxidation in freeze-thawed bighead carp (Hypophthalmichthys nobilis) fillets using silver carp (Hypophthalmichthys molitrix) fin hydrolysates. *LWT, 123*, Article 109050.
Zhang, Y., Chen, S., Qi, B., Sui, X., & Jiang, L. (2018). Complexation of thermally-denatured soybean protein isolate with anthocyanins and its effect on the protein structure and in vitro digestibility. *Food Research International, 106*, 619–625.
Zhu, J., Li, L., Zhao, L., Song, L., & Li, X. (2019). Effects of freeze–thaw cycles on the structural and thermal properties of wheat gluten with variations in the high molecular weight glutenin subunit at the Glu-B1 locus. *Journal of Cereal Science, 87*, 266–272.
Zhu, X. F., Zheng, J., Liu, F., Qiu, C. Y., Lin, W. F., & Tang, C. H. (2018). Freeze-thaw stability of Pickering emulsions stabilized by soy protein nanoparticles. Influence of ionic strength before or after emulsification. *Food Hydrocolloids, 74*, 37–45.